Fig. 1 RWL-3000 servo-controlled testing machine

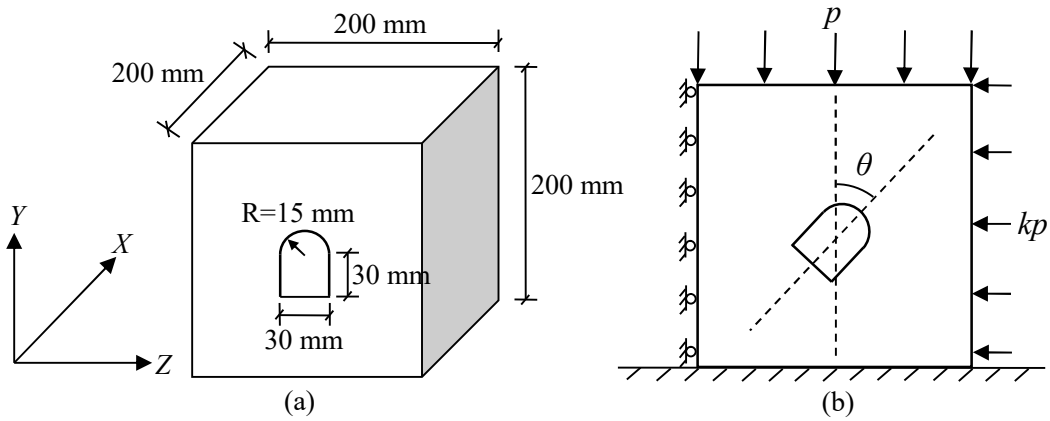

Fig. 2 The physical model (a) model size and (b) loading conditions

(a) Physical models made of cement mortar

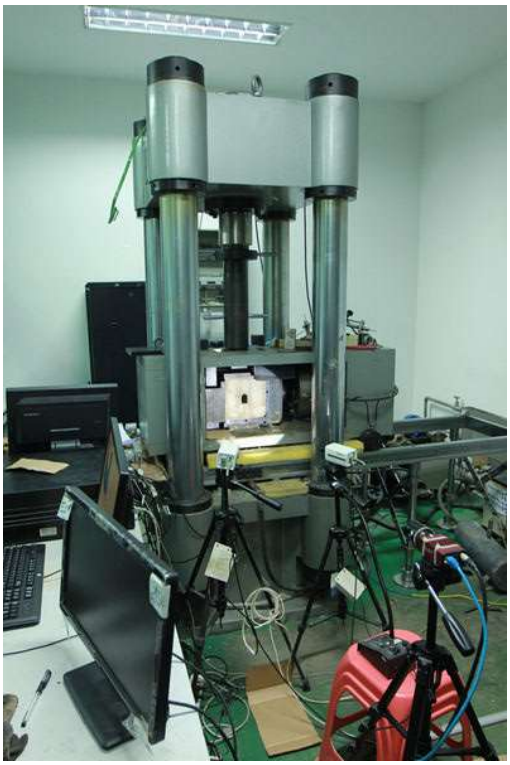

(b) Loading process

Fig. 3 Physical models and loading process

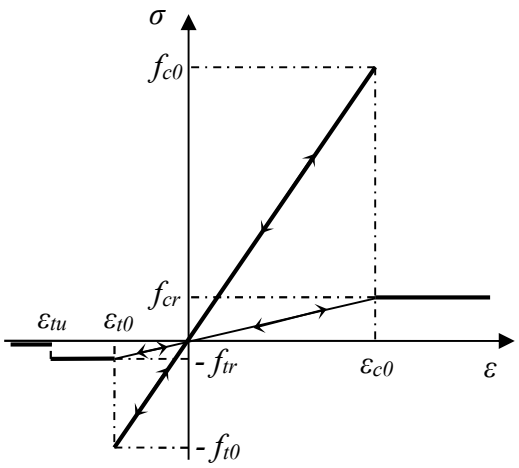

Fig. 4 Constitutive relation of an element under uniaxial stress state

$\theta = 0°$ $\theta = 15°$ $\theta = 30°$

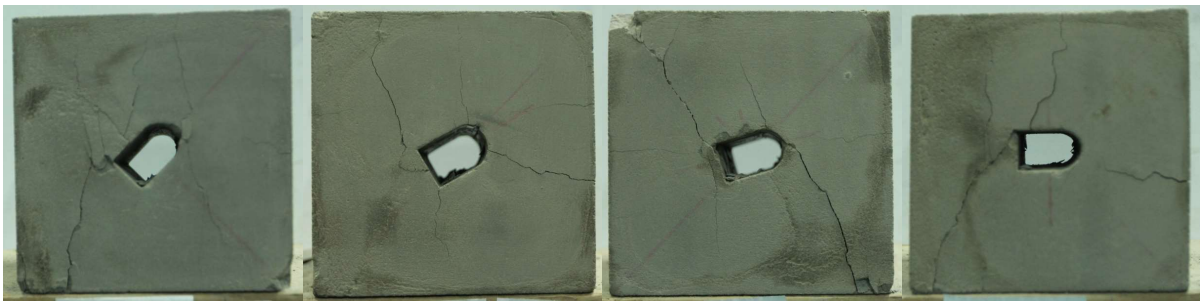

$\theta = 45°$ $\theta = 60°$ $\theta = 75°$ $\theta = 90°$

Fig. 5 Failure modes when the lateral pressure coefficient k = 0.125

$\theta = 0°$ $\theta = 15°$ $\theta = 30°$

$\theta = 45°$ $\theta = 60°$ $\theta = 75°$ $\theta = 90°$

Fig. 6 Failure modes when the lateral pressure coefficient $k = 0.5$

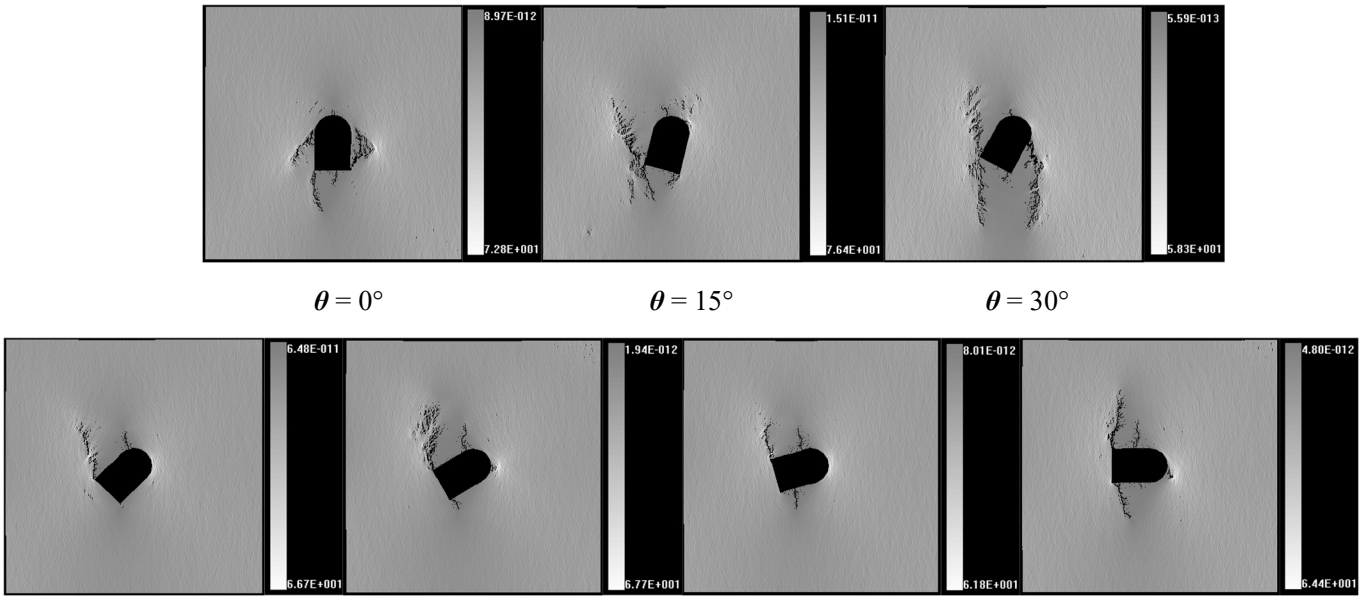

$\theta = 0°$ $\theta = 15°$ $\theta = 30°$

$\theta = 45°$ $\theta = 60°$ $\theta = 75°$ $\theta = 90°$

Fig. 7 Shear stress contour when the lateral pressure coefficient k = 0.125 by simulation (Unit: Pa)

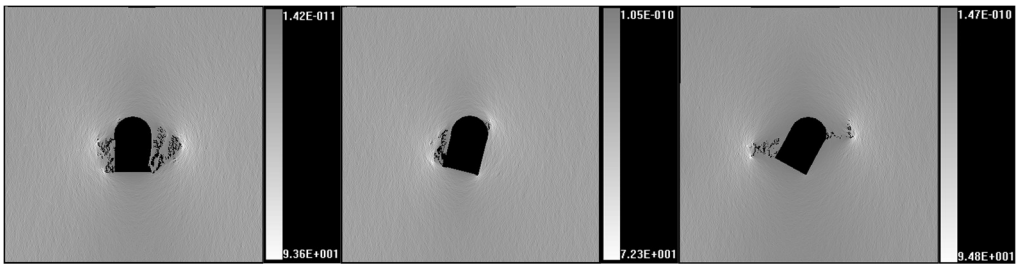

$\theta = 0°$ $\theta = 15°$ $\theta = 30°$

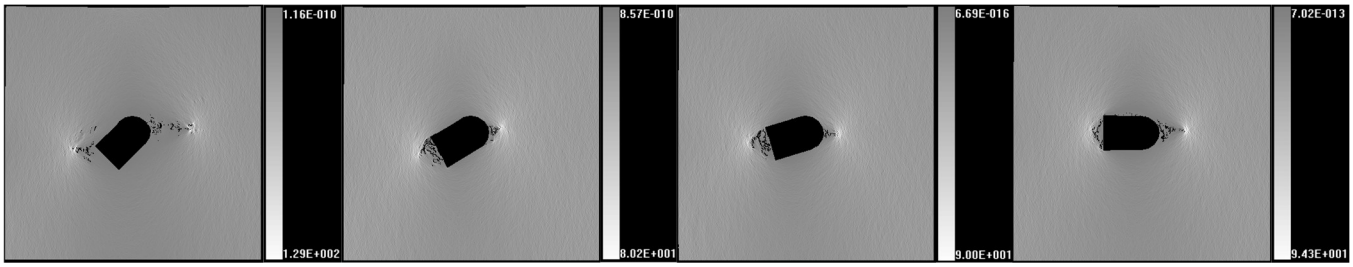

$\theta = 45°$ $\theta = 60°$ $\theta = 75°$ $\theta = 90°$

Fig. 8 Shear stress contour when the lateral pressure coefficient k = 0.5 by simulation (Unit: Pa)

(a) k = 0.125

(b) k = 0.25

(c) k = 0.5

(d) k = 0.75

Fig. 9 Failure modes with the lateral pressure coefficient k changing

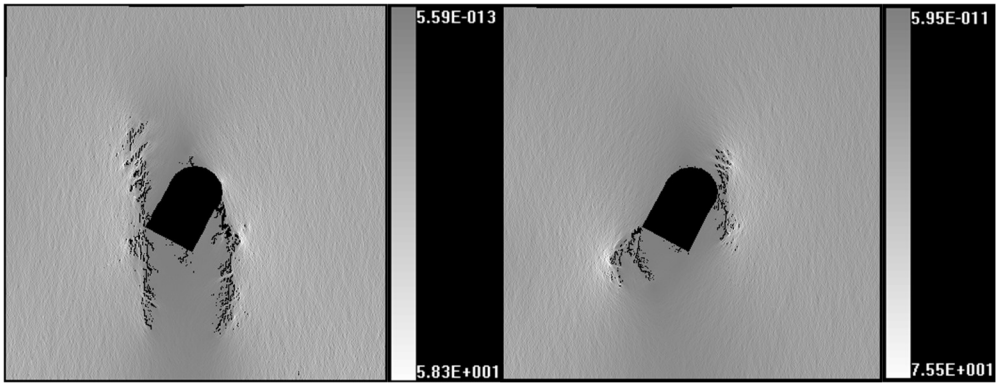

(a) k = 0.125 **(b) k = 0.25**

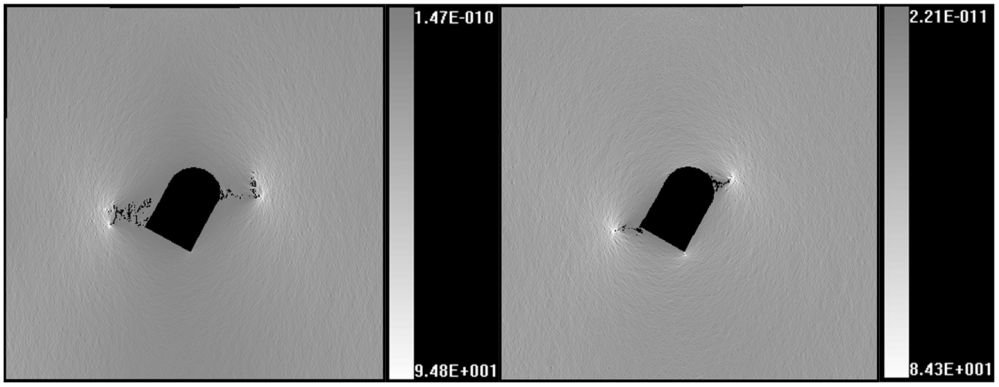

(c) k = 0.5 **(d) k = 0.75**

Fig. 10 Shear stress contour with the lateral pressure coefficient k changing by simulation (Unit: Pa)

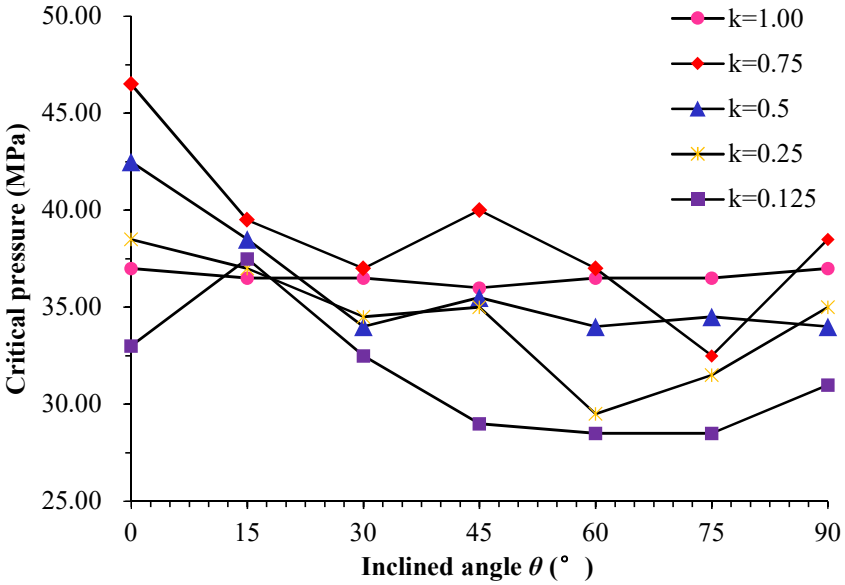

Fig. 11 Critical pressure curves of horseshoe-shaped tunnel model